Journal of Magnetic Resonance **148,** 277–288 (2001)
doi:10.1006/jmre.2000.2252, available online at http://www.idealibrary.com on IDEAL®

Iterative Lineshape Analysis of Quadrupolar Echo Spectra of a Damped CD_3 Quantum Rotor: Preliminary Evidence of a Novel Mechanism of Stochastic Spin Exchange

S. Szymański,*,[1] Z. Olejniczak,† A. Detken,‡,[2] and U. Haeberlen‡

*Institute of Organic Chemistry, Polish Academy of Sciences, Kasprzaka 44/52, 01-224 Warsaw, Poland; †Institute of Nuclear Physics, Radzikowskiego 152, 31-342 Kraków, Poland; and ‡Max-Planck-Institut für Medizinische Forschung, Jahnstrasse 29, 69120 Heidelberg, Germany

Received April 26, 2000; revised September 19, 2000

It is demonstrated that the wealth of information about damped quantum rotation of CD_3 groups, contained in quadrupolar echo spectra, can be fully explored in a broad temperature range using a method of iterative analysis of the spectral lineshapes. The recently reported lineshape equation which, apart from the quantum tunneling and the dissipative Alexander–Binsch terms, contains an additional dissipative term having no classical analog is shown to be capable of describing even subtle details of the spectra of a crystal of acetylsalicylic acid–CD_3 oriented specifically in the magnetic field. Preliminary evidence of the occurrence of this novel dissipative mechanism in the system studied is reported. The results obtained seem to suggest that there is no "classical limit" in the dissipative behavior of this system.

INTRODUCTION

Quantum rotation in solids at cryogenic temperatures has been a subject of NMR investigations since the late 1960s. The current trends in and the history of the NMR research involving the methyl group rotation has just been extensively reviewed (*1*). Due to the progress in NMR studies on single crystals that was achieved in the recent decade, now even subtle details of the fine structure of the tunneling patterns are experimentally accessible (*2–7*). This is particularly true for CD_3 rotors whose ^2H resonances are not so much broadened by spin–spin interactions as for protonated species. Effects of the coherent tunneling on the NMR spectra of deuterated methyl groups are now well understood (*3*, *8*). The situation is less clear for the lineshape phenomena which evolve gradually with increasing temperature and reflect accelerated damping of the coherent motion of the rotor under impact of its condensed environment. A preliminary quantum mechanical description of such effects, involving CD_3 rotors with very large tunneling frequencies, was proposed by Heuer (*9*). A general theory, developed in a similar spirit, but free of such a limitation and covering the protonated systems as well, has been reported recently (*10*). In the present contribution, the NMR lineshape equation derived in the latter work is confronted with the experimental spectra of the CD_3 group in a crystal of selectively deuterated acetylsalicylic acid, measured up to temperatures where the incoherent processes dominate over the coherent tunneling. In our previous study on the same model system (*4*), the spectra were measured using both the free induction decay (FID) and the quadrupolar echo (QE) techniques (*11*). The theoretical interpretation of the observed QE patterns was, however, confined to the low-temperature limit where the incoherent effects could be neglected. The latter work provides evidence of some advantages of the QE technique over the FID experiment in studies on tunneling CD_3 groups. These include: (i) the elimination of baseline distortions that normally occur in the FID spectra covering broad resonances and (ii) a substantial amplification of some relevant details of the fine structure which are barely visible in the FID spectra. The experimental QE spectra described in the present work were remeasured following the procedures described previously (*4*) and using the same NMR facilities. The FID spectra were remeasured using radiofrequency pulses with exactly the same parameter settings as in the QE experiments.

THEORY

Below, a brief recapitulation of the relevant results of Ref. (*10*) is given. The dynamic model adopted therein, which is depicted schematically in Fig. 1, involves a YX_3 quantum rotor embedded in a condensed environment acting as a thermal bath. The rotor–bath interactions lead to vibrational relaxation within the manifold of the torsional states of the rotor. Due to restrictions imposed on the thermal transitions by the symmetrization postulate of quantum mechanics, the relaxation processes that generally fall in the picosecond range are inefficient with respect to some specific coherences between the torsional sublevels. For methyl groups, for which the rigid-rotor approximation is adequate, these sublevels come in triplets whose

[1] To whom correspondence should be addressed. E-mail: sszym@icho.edu.pl.
[2] Present address: Laboratorium für Physikalische Chemie, ETH Zentrum, CH-8092 Zürich, Switzerland.

1090-7807/01 $35.00

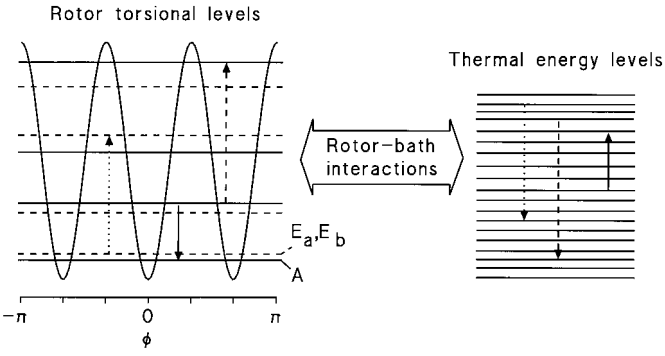

FIG. 1. The dynamic model of a methyl-like quantum rotor in contact with thermal bath, adopted in Ref. (*10*). The rotor–bath interactions affect the torsional coordinate, ϕ, only; accordingly, they do not couple the torsional states of different symmetries $\Gamma = A$, E_a, and E_b. The fast vibrational relaxation processes induced in this way within the rotor system spare certain quantum mechanical coherences engaging pairs of the torsional sublevels at the individual torsional levels. For each pair of symmetry labels Γ and Γ' there is only one such coherence that is sufficiently long-lived to be observable on the NMR time scale. The long-lived coherences (E_a, E_b) $((E_b, E_a))$ are damped with the rate constant k_K and (E_a, A) and (E_b, A) $((A, E_a)$ and $(A, E_b))$ with rate constant k_t. The oscillation frequency, Δ $(-\Delta)$, of the latter is a temperature-dependent average of the tunneling splittings at the sequential torsional levels; the oscillation frequency of the former is zero.

individual components transform as the respective symmetry species, A, E_a, and E_b, of the cyclic group C_3 (which describes the intrinsic symmetry of the system in configuration space rather than the geometric symmetry of the rotor—the latter can be nonsymmetric). It is these long-lived coherences that are observed in NMR experiments on tunneling methyl groups. The spin-space correlations due to the symmetrization postulate allow one to project the dissipative rotor dynamics solely onto the spin manifold. The effective equation of motion for the spin density matrix, $\hat{\rho}$, of the X and Y nuclei, obtained in this way reads:

$$d\hat{\rho}(t)/dt = -\frac{i}{\hbar}\left[\hat{H}_Z + \hat{H}_D + \hat{H}_Q - \frac{h\Delta}{3}(\hat{P} + \hat{P}^{-1}),\ \hat{\rho}(t)\right] - \frac{4k_t - k_K}{36}[\hat{P} + \hat{P}^{-1}, [\hat{P} + \hat{P}^{-1},\ \hat{\rho}(t)]] - \frac{k_K}{12}[\hat{P} - \hat{P}^{-1}, [\hat{P}^{-1} - \hat{P},\ \hat{\rho}(t)]], \quad [1]$$

where none of the operators is dynamically dependent on the spatial coordinates of the tunneling particles. In Eq. [1], the symbols $\hat{H}_I$ $(I = Z, D, Q)$ designate the effective Zeeman, dipolar, and quadrupolar spin Hamiltonians, respectively, and $\hat{P}$ represents cyclic permutation of the spin variables of the X_3 unit. The rate constant k_K entering Eq. [1] describes damping of the unique quantum coherence which engages pairs of the torsional sublevels E_a and E_b (the Kramers pairs) and which is spared by the rapid vibrational relaxation processes. The rate constant k_t is an analog of k_K involving the (only) long-lived coherence between the sublevels of symmetry A and any of the Kramers sublevels; this unique coherence oscillates with frequency Δ which is a quantum-statistical average (but, in general, with non-Boltzmann weights) of the tunneling splittings at the sequential torsional levels. The quantities k_K and k_t can be identified (*10*) with the half-width-at-half-height of the quasielastic and inelastic lines, respectively, in the inelastic neutron scattering (INS) spectra of YH_3 rotors; the quantities $\pm h\Delta$ are the energy shifts of the inelastic Stokes and anti-Stokes lines (*9*, *12–14*). The total Hamiltonian in the first commutator of Eq. [1] is just the long-known effective spin Hamiltonian of Apaydin and Clough (*15*). However, outside the low-temperature limit not only the tunneling frequency, Δ, but also the Larmor frequencies, the dipole–dipole, and the quadrupole coupling constants, which enter its respective terms as parameters, are all quantum-statistical averages over the torsional ladder of the pertinent dynamic variables in the exact Hamiltonian. In extreme situations, e.g., for torsional potentials with flat minima, the familiar $[3\cos^2\theta - 1]$-angular dependences of second-rank tensorial interactions may only approximately be valid. In what follows, we abandon assumptions about a particular angular dependence of the effective quadrupolar Hamiltonian in Eq. [1] as well as about possible (C_3) symmetry relationships between the EFG tensors at the individual deuteron sites. Instead, it will be parametrized in terms of three effective quadrupolar coupling constants, q_A, q_B, and q_C, corresponding to the three equilibrium sites of the deuterons in a given orientation of the CD_3 group relative to the external magnetic field. These effective quantities are normalized in such a way that the secular part of the quadrupolar Hamiltonian, which is the only relevant part in the present context, can be written as

$$\hat{H}_Q = \frac{h}{4}\sum_{D=A,B,C} q_D[3\hat{I}_{zD}^2 - I(I+1)]. \quad [2]$$

The form of the dissipative terms in Eq. [1] may suggest that the equation remains valid only as long as $k_t > k_K/4$. Such a proviso was actually made in Ref. (*10*). It will be shown later on that this is a needless restriction, and the validity of Eq. [1] is retained for any values of k_t and k_K. These dissipative terms can be formulated in several equivalent ways. In the present context, of particular interest will be the following form:

$$-\frac{k_K}{3}[2\hat{\rho}(t) - \hat{P}\hat{\rho}(t)\hat{P}^{-1} - \hat{P}^{-1}\hat{\rho}(t)\hat{P}] - \frac{k_t - k_K}{2}[\hat{\rho}(t) - \hat{U}\hat{\rho}(t)\hat{U}], \quad [3]$$

where

$$\hat{U} = \frac{1}{3}[\hat{1} - 2(\hat{P} + \hat{P}^{-1})] \qquad [4]$$

is a unitary, self-inverse matrix. In the formulation of Eq. [3], the term proportional to k_K can easily be recognized to be the familiar Alexander–Binsch (AB) term (*16, 17*) which was originally introduced to describe effects of classical exchange, or random jumps, in spin-coupled systems of like, nonisochronous nuclei. However, for a tunneling methyl group one can only speak about pseudo-classical jumps, because such jumps may occur via activated incoherent tunneling (*10*). As to the remaining term, that proportional to $k' = k_t - k_K$, in the instances where $k_t \geq k_K$ (which inequality seems to be generally fulfilled by the corresponding quantities in the INS spectra of protonated methyl groups (*18, 19*)) its very form also calls for an interpretation in terms of random jumps of some sort, ones represented by the unitary operator $\hat{U}$. Since the latter describes transformation from a localized to a specifically delocalized state of the rotor (or vice versa, for $\hat{U}^2 = \hat{1}$) (*10*), such jumps can have no classical analogs. The question of a more precise interpretation of such nonclassical exchange terms must currently be left open. At the end of the present section we will only see that a formulation of the dissipative part of Eq. [1] exclusively in terms of nonclassical jump operators of the above sort affords immediate evidence of a general validity of that equation.

Below, we consider effects of the dissipative terms, using the formulation of Eq. [3], on the lineshapes of CD_3 rotors in the limit of a large tunneling frequency. The structure of deuteron spectra of such systems in the absence of dissipation was discussed in detail in Ref. (*3*). The limiting spectral patterns for two different orientations of the rotor in the external magnetic field are displayed in Fig. 2. The quantities $|\alpha|$ and β describing these limiting patterns were defined previously under the assumption that the EFG tensors at the individual deuteron sites obey C_3 symmetry. Redefined in terms of the effective quadrupolar coupling constants of Eq. [2], these two quantities are

$$\beta = \frac{1}{4}(q_A + q_B + q_C)$$

$$\alpha = \frac{1}{4}(q_A + \epsilon q_B + \epsilon^* q_C), \qquad [5]$$

where $\epsilon = \exp(2\pi i/3)$. The parameter $|\alpha|$ is a synthetic measure of the differences between the magnitudes of the effective quadrupolar coupling constants; for the orientations where $|\alpha|$ is of the order of the natural line broadenings, practically no information about the rotor dynamics is contained in the spectra.

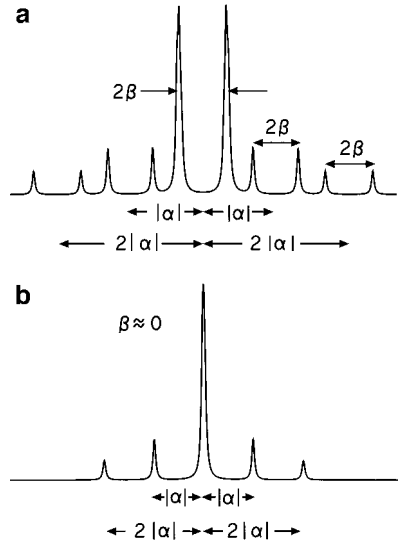

FIG. 2. Simulated low-temperature FID spectra of a CD_3 group with perfect tetrahedral symmetry, for a tunneling frequency of 3 MHz; axial symmetry is assumed for the EFG tensors at the individual equilibrium deuteron sites, with the unique principal axes directed along the respective C–D bonds. Quadrupolar coupling constants of 170 kHz were assumed for the individual deuterons. Orientations of the external magnetic field are described by the polar angles Θ and ϕ of 72 and $-84°$, respectively, in (a), and of 55 and $-97°$, respectively, in (b), in the molecular frame whose z axis is parallel to the C_3 axis and points to the rest of the molecule, while the x axis points along the projection of a C–D bond onto the plane perpendicular to z. The quantities α and β are defined in the text.

In the limit of $|\alpha|/\Delta \ll 1$, the properties of the Apaydin and Clough Hamiltonian in Eq. [1] can be discussed using a spin basis set adapted to C_3 symmetry. In this limit, the Hamiltonian matrix elements that connect basis states of symmetry A with basis states of symmetries E_a and E_b become strongly nonsecular and can be neglected. Accordingly, the eigenstates can be classified as pure A states or combinations of E_a and E_b states, that is, as E states in brief (*3, 9*). Of the transitions shown in Fig. 2, those at $\pm|\alpha| \pm \beta$ and $\pm 2|\alpha| \pm \beta$ (the "α" transitions) are pure EE transitions, while each of the lines at the frequencies $\pm\beta$ (the "β" lines) is a superposition of pure AA transitions and pure EE transitions (in 5 to 1 proportion). Transitions between eigenstates of different symmetries, that is, AE and EA, have nearly zero intensity and occur far in the wings, in the frequency regions around $\pm\Delta$. Now, one can easily see that the dissipative term in Eq. [3] which is proportional to $k_t - k_K$, or the nonclassical term, has no effect on the pure AA and pure EE transitions (note that $\hat{U}|\Gamma i\rangle\langle\Gamma j|\hat{U}^{-1} = |\Gamma i\rangle\langle\Gamma j|$ for any pair of eigenstates i and j of symmetry $\Gamma = A, E$). This term can only affect transitions AE and EA, but these fall far beyond the frequency region normally observed. On the other hand, the dissipative term proportional to k_K, or the pseudo-classical term, spares only the pure AA transitions, while it can potentially affect all of the remaining transitions. Accordingly, in the limit of large Δ, the bath-induced processes will cause broadenings, coalescences, and, eventually, mo-

tional narrowings of the *EE* resonances. These effects will be particularly strongly reflected in the shapes of the α lines, while the *AA* lines at $\pm\beta$ will remain unaffected. The above reasoning remains valid as long as $\Delta \gg k_K, k_t$. An essentially equivalent description of the lineshape effects in the limit defined above is given by the already quoted Heuer theory (*9*).

When the inequality $|\alpha|/\Delta \ll 1$ becomes weaker, the eigenstates of the Apaydin and Clough Hamiltonian lack their pure *A* and pure *E* properties. Still, the modified eigenstates will bear either a dominating *A* or a dominating *E* character. In other words, the former pure *EE* and *AA* transitions will now each contain admixtures of the *EA* and *AE* transitions (to second order in $|\alpha|/\Delta$, there is no mixing of *AA* and *EE* transitions). A further reasoning based on second-order perturbation calculations reveals that these effects will be most pronounced for the intense *AA* singlets at the frequencies $\pm\beta$, which will now be turned into multiplets, and effectively into triplets, with the splittings being of the order of $|\alpha|^2/\Delta$. Owing to the admixture of the *AE* and *EA* transitions, the individual components of such multiplets will now become sensitive to both the pseudo- and the nonclassical dissipative processes. Normally, Δ decreases as the temperature is increased so that the contribution of the latter transitions to the β multiplets increases with temperature. Numerical simulations reported in Ref. (*10*) confirm that, indeed, at elevated temperatures the impact of the nonclassical process on the lineshapes of these multiplets can be quite substantial. However, if it happens that in the temperature range where the spectra are sensitive to the latter process the difference between k_t and k_K becomes small, the nonclassical effects can easily be overlooked. This may be the reason why the occurrence of such effects has not been noticed so far.

It is clear that the dissipative terms in Eq. [1] cannot mix transitions (and, precisely, coherences) from different symmetry manifolds $\{AA\}$, $\{EE\}$, $\{AE\}$, and $\{EA\}$. Exploiting the latter property, one can also explain the NMR behavior of any methyl-like system in the instance where the rate constants k_K and k_t are much larger than $|\alpha|$ while Δ can be of any magnitude. This could especially be suited to discussing the NMR lineshapes of CD_3 rotors in the high-temperature limit. This somewhat intricate problem, having immediate consequences for the spin relaxation theory, will be addressed under a separate cover. In the present contribution, we only mention that in considering the high-temperature behavior one must take into account the possibility that the rate constant k' can turn into a negative, which would undermine the significance of not only the nonclassical but also the pseudo-classical (AB) terms.

As has already been mentioned, a general formulation of the stochastic part of Eq. [1], bringing out the dissipative character of the latter for any values of k_K and k_t, can be arrived at at the cost of abandoning the notion of pseudoclassical jumps. Instead, one can introduce two more sorts of nonclassical jumps, described by unitary selfinverse matrices $\hat{V}$ and $\hat{V}^*$ which are close analogs of $\hat{U}$, namely,

$$\hat{V} = \frac{1}{3}[\hat{1} - 2(\epsilon\hat{P} + \epsilon^*\hat{P}^{-1})]. \quad [6]$$

Like $\hat{U}$, each of these matrices represents a unitary transformation of a localized state of the rotor into a specifically delocalized state of the latter (or vice versa). Now, the pertinent terms in Eq. [1] can be rearranged in such a way that the contributions of the rate processes described by k_K and k_t are separated, that is,

$$-\frac{k_K}{4}[\hat{\rho}(t) + \hat{U}\hat{\rho}(t)\hat{U} - \hat{V}\hat{\rho}(t)\hat{V} - \hat{V}^*\hat{\rho}(t)\hat{V}^*] - \frac{k_t}{2}[\hat{\rho}(t) - \hat{U}\hat{\rho}(t)\hat{U}]. \quad [7]$$

The dissipative character of the term proportional to k_t for any (positive !) value of k_t is now evident. In order to show the same property for that proportional to k_K, we first note that the product of any two of the three (mutually commuting) unitary matrices $\hat{U}$, $\hat{V}$, and $\hat{V}^*$ entering that term gives the remaining matrix with minus sign, $\hat{U}\hat{V} = -\hat{V}^*$, $\hat{U}\hat{V}^* = -\hat{V}$, and $\hat{V}\hat{V}^* = -\hat{U}$. Therefore, the set of their Kronecker products, $\hat{U} \times \hat{U}^*$ $(= \hat{U} \times \hat{U})$, $\hat{V} \times \hat{V}^*$, and $\hat{V}^* \times \hat{V}$, which are the Liouville space transcripts of the respective unitary transformations on $\hat{\rho}$ entering the first term in Eq. [7], augmented with the unit transformation $\hat{1} \times \hat{1}$, form an Abelian, four-element group. Accordingly, the entire term can in Liouville representation be expressed as a (unnormalized) group-superprojection on the supervector $|\rho\rangle\rangle$, where the superprojector is concerned with the irreducible representation in which the group elements $\hat{1} \times \hat{1}$ and $\hat{U} \times \hat{U}$ are represented by 1 and those $\hat{V} \times \hat{V}^*$ and $\hat{V}^* \times \hat{V}$ by -1. Therefore, the term under discussion retains its dissipative character for any value of k_K since for any such (positive !) value it is represented by a negative (semi-)definite matrix. Therefore, the restriction of Ref. (*10*) limiting the range of validity of Eq. [1] to the instances where $k_t \geq k_K/4$ is immaterial; in reality, it involves one of the possible ways of interpretation of the stochastic terms in that equation.

In the sequel we will use the formulation of Eq. [3] for these terms, because this specific formulation will facilitate a comparison of the results obtained currently with those reported earlier (*5*). Possible ambiguities regarding the concepts of nonclassical jumps will be avoided in what follows, because any reference to a nonclassical dissipative process will from here on involve the nonclassical jump process defined in Eq. [3], regardless of whether its corresponding rate parameter, k', is positive or negative. The fact that, as we shall see later on, the latter possibility may actually be encountered in practice can serve as a warning against taking the interpretations of both of the exchange terms in Eq. [3] too literally.

Equation [1] with only the AB term retained has already been applied to interpret ^2H and ^{13}C FID spectra of several

damped methyl rotors (*5–7*). No systematic attempts have so far been made to use its full version to interpret experimental spectra of methyl groups. In the present study, an iterative least-squares fitting algorithm based on Eq. [1] is used to compare the theoretical and experimental lineshapes of both QE and FID spectra of the single-crystal sample mentioned in the Introduction. The spectra analyzed in the present study were measured for two orientations, I and II, of the crystal, for which the limiting low-temperature spectra resemble the prototype patterns in Figs. 2a (I) and 2b (II). Precise characteristics of these orientations are given in the legends to Figs. 6 (I) and 5 (II) in Ref. (*4*). It ought to be mentioned here that for each of these orientations the external magnetic field is parallel to the monoclinic plane of the crystal (whose space group is $P2_1/c$ (*20*)), which renders both CD_3 groups in the elementary cell magnetically equivalent (*3*).

COMPUTATIONAL DETAILS

The lineshape of a QE spectrum measured following the procedure described previously (*4*) can be concisely described using the Liouville space notation, namely,

$$M(\omega) \propto \left\langle\left\langle F_+ \left| \exp\left[\left(-i\mathbf{L}' + \mathbf{X} - \frac{1}{2\pi T_2^*}\mathbf{1}\right)(\tau + \delta_e)\right]\right.\right. \times \left[-i(\mathbf{L} + \omega 1) + \mathbf{X} - \frac{1}{2\pi T_2^*}\mathbf{1}\right]^{-1} \times \mathbf{\Pi}_u \exp\left[\left(-i\mathbf{L}' + \mathbf{X} - \frac{1}{2\pi T_2^*}\mathbf{1}\right)\tau\right] \times \left.\left.\mathbf{\Pi}_{u\pm\pi/2}\left|F_z\right\rangle\right\rangle\right\rangle, \quad [8]$$

where the superoperator representing a radiofrequency pulse of duration τ_p and amplitude ω_1 applied along axis $u = \pm x$ or $\pm y$ of the frame rotating with an average Larmor frequency of the ^2H nuclei is given by

$$\mathbf{\Pi}_u = \exp\left\{\left[-i(\omega_1 \mathbf{F}_u^D + \mathbf{L}') + \mathbf{X} - \frac{1}{2\pi T_2^*}\mathbf{1}\right]\tau_p\right\}, \quad [9]$$

with $\mathbf{F}_u^D$ denoting the commutator $[\hat{F}_u,]$. As described previously (*4*), the pulse settings were carefully adjusted to emulate ideal $\pi/2$, on-resonance pulses, which is crucial for obtaining nondistorted QE spectra. In Eq. [8] $\mathbf{L}$ is the super-Hamiltonian, expressed in angular frequency units, generated by the Hamiltonian of Eq. [1] in which only the secular parts of $\hat{H}_Q$ and $\hat{H}_D$ (the parts which commute with $\hat{F}_z$) are retained, and $\mathbf{L}'$ is the part of $\mathbf{L}$ which is time-independent in the rotating frame; X collectively denotes the dissipative terms in Eq. [1]. The refocusing time after which the maximum of the echo is observed must be set longer by an increment δ_e (of the length of a few microseconds (*4*)) than the echo time, τ, because of an instrumental delay.

In measuring the FID spectra, the NMR signal following the stimulating pulse was processed according to the procedure described previously (*4*). In the cases where there are no resonances far in the wings, a fair theoretical description of the FID spectra obtained in the above way can be made using a simplified version of Eq. [8] in which the exponential superoperators as well as the superoperator representing the second pulse are omitted. If the spectral width becomes comparable with $1/\tau_p$, which takes only place in the low-temperature limit, a reasonable approximation is to eliminate from Eq. [8] the first exponential and the second pulse superoperators, while the refocusing superoperator is still retained. In the latter superoperator, the dissipative part can be neglected (the dissipation is slow at low temperatures) and the refocusing time $\tau + \delta_e$ is to be replaced by an adjustable (see below), *negative* time increment δ_f whose magnitude ought to be roughly equal to $\tau_p/2$. This is an approximate description of the operation of an optimal localization of the time origin of the NMR signal which is an essential ingredient of the procedure quoted above, introduced in order to minimize frequency-dependent phase distortions. The errors introduced in this way are much smaller than in the case where an ideal RF pulse (i.e., one of infinitely short duration) was assumed in the calculations of the FID spectra.

In both FID and QE experiments, appropriate phase cycling schemes were employed to eliminate channel unbalance and, in the QE experiments, the impact of even-order coherences that arise after the first RF pulse due to pulse imperfections and are then turned into an observable NMR signal by the second pulse.

A FORTRAN computer program was written to calculate both FID and QE spectra according to Eq. [8], with an account of the appropriate phase cycling. The (super)matrices entering the equation have dimensions of 729×729 and are too large to be handled efficiently. They were therefore factored into independent blocks of smaller dimensions by exploiting some of their natural symmetries. The block-diagonalization of the individual superoperators in the exponentials and in the rectangular brackets in Eq. [8] was achieved by exploiting commutation properties of all of these operators with the set of mutually commuting superoperators $\mathbf{F}_z^D$, $\mathbf{F}_z^L$, and $\mathbf{F}_z^R$ (the two latter are the left- and right-translation components, respectively, of $\mathbf{F}_z^D$). Neglect of the dipole–dipole interactions between the ^2H nuclei would result in a further increase of the symmetry of the superoperators involved. However, as will further be commented upon in the sequel, intramolecular dipolar interactions are generally relevant and cannot be neglected in the above context. On the other hand, they are totally irrelevant in calculating the pulse superoperators. In the latter context, the possible off-resonance shift of the pulse frequency, which might still be left despite careful pulse adjustments, can also be safely neglected. With both of these two (small) terms

neglected, the superoperators entering the exponential in Eq. [9] simultaneously commute with the set of mutually commuting superoperators $\mathbf{Q}_u^{\mathrm{D}}$, $\mathbf{Q}_u^{\mathrm{L}}$, and $\mathbf{Q}_u^{\mathrm{R}}$, where $\hat{Q}_u = \sum_{D=A,B,C} \hat{I}_{uD}^2$. As a result of these commutation properties, the largest block that had to be handled in calculating the pulse superoperators was only of the dimensions of 144×144 and of the dimensions of 42×42 at the stage of calculating the spectrum at the desired frequencies.

The routine to calculate the QE and FID spectra was employed in a least-squares minimization program based on the Gauss–Newton iterative algorithm. The derivatives entering the Hessian matrix were approximated by the corresponding quotients of finite increments. The minimization program was designed to be capable of handling a number of QE and FID spectra simultaneously. Actually, the input data for a single minimization run can include up to nine spectra measured at a given temperature for a given orientation of the crystal in the magnetic field. Owing to such a policy, essentially no convergence problems were encountered despite a large number of parameters being fitted simultaneously. The parameter set includes three "local" parameters for each of the input spectra: the amplitude factor, the baseline position, and the shift of the frequency axis of the given spectrum relative to the origin of a common frequency scale (for the FID spectrum, also the parameter δ_{f}). Beyond that, it includes "global" parameters, of which each can potentially affect the lineshapes of all of the spectra. Among these global parameters there are two of the adjustable instrumental parameters: the pulse amplitude, ω_1, and the time delay δ_{e}. The global parameters of central interest in the present study include the effective tunneling frequency, Δ, the damping-rate constants k_K and $k' = k_t - k_K$, and, for each of the two crystal orientations, the corresponding set of three effective quadrupolar coupling constants, q_A, q_B, and q_C. In the course of data handling it came out that some impurity signals visible in the spectra had also to be accounted for in the calculations. These signals are typical quadrupolar doublets with no features due to tunneling. The set of global parameters had to be augmented by lineshape parameters of two such doublets (the lineshapes of the impurity signals were calculated assuming ideal pulses). It had also to be augmented by the "natural" line broadening $1/\pi T_2^*$, and, for one of the two orientations of the crystal, by an effective dipole coupling constant between the deuterons within the CD_3 group, d_{eff}.

RESULTS AND DISCUSSION

In the previous NMR studies on acetylsalicylic acid-CD_3 (*3, 5*), basic characteristics of the tunneling system were determined by the combined use of several NMR techniques, including a visual comparison of the experimental and simulated FID spectra. The parameters entering the quadrupolar Hamiltonian were determined under assumptions that, first, the EFG tensors at the individual deuteron sites are axially symmetric, and second, the corresponding three principal directions are related by a perfect threefold symmetry. The validity of these assumptions was further confirmed in the studies on partially protonated CH_nD_{3-n} groups (*21–23*). It was tempting to check whether the relevant system parameters could be evaluated directly from spectra, without any simplifying assumptions and in a possibly most objective way. We first tried to apply the minimization routine described above to the individual FID and QE spectra, but then convergence problems were often encountered, and the results obtained from spectra measured at the same temperature were sometimes inconsistent. The policy of analyzing simultaneously the whole sets of spectra measured under given experimental conditions has proven much more effective, despite large sets of parameters that had to be fitted.

The sets of FID and QE spectra, each including one FID and eight QE spectra, were measured in the temperature range of 22 to 50 K; for orientation I, the measurements were also performed at 17 K. In the low-temperature limit, that is, up to 26 K in our case, the fine structure of the α lines is still visible. Above 34 K, the spectral patterns lack any fine structure; the fits were performed only for the experiments below 36 K. The information content in the spectral lineshapes diminishes gradually along with increasing temperature. The computational strategy had to be modified accordingly on passing to the intermediate- and high-temperature regions. The relevant details of the calculations are discussed below.

In the low-temperature limit, together with the system parameters, it was also possible to determine the experimental parameters δ_{f}, δ_{e}, and ω_1. As expected, the obtained values of δ_{f} are negative. For orientation I and II they are approximately equal to one-half and one-third, respectively, of the pulse duration $\tau_{\mathrm{p}} = 2.3$ μs. For both orientations, the optimized magnitude of δ_{e} is about 1.8 μs, again in agreement with the expectations. The optimized magnitude of $\omega_1/2\pi$ amounts to 108.2 kHz for orientation II and 105.2 kHz for orientation I. In the analysis of spectra from temperatures above 26 K, the parameters δ_{e} and ω_1 were kept fixed (as has already been mentioned, in calculating the FID spectra, the term dependent on δ_{f} was neglected). The results obtained for the above experimental parameters confirm that the theoretical model of the QE experiment, displayed in Eq. [8], is realistic.

The intramolecular dipolar interactions between the deuterons, calculated assuming the standard geometry of a methyl group, small as they are, were nevertheless accounted for in the lineshape equation. For orientation II, the lineshape fits were repeated for the dipolar coupling constant, d_{eff}, varied in reasonable limits, and the obtained results were practically the same. A different behavior was observed for orientation I where optimization of d_{eff} was possible (see below).

As is seen from Eq. [8], for all of the resonances in D_3 the natural lineshape was assumed to be a Lorentzian of the width $w = 1/\pi T_2^*$. This approximation is probably not unrealistic in view of the quality of the obtained fits, especially for orientation II. In the analysis of the spectra for temperatures up to 30

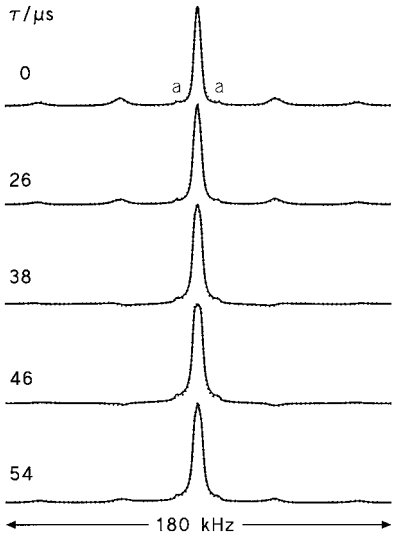

FIG. 3. Selected experimental QE spectra of acetylsalicyclic acid–CD_3 (solid lines) and the corresponding theoretical "best fit" spectra (dotted lines) for the displayed values of echo time ($\tau = 0$ designates the FID spectrum), for orientation II at 24 K. The label *a* describes an impurity doublet. The values (in kilohertz) of the effective quadrupolar coupling constants q_A, q_B, and q_C obtained at convergence are -67.5 ± 0.3, 81.7 ± 0.2, and -13.1 ± 0.5, respectively. For the pertinent orientation parameters Θ and ϕ listed in the legend to Fig. 2, the values calculated from the previous estimates, based on the assumption that the properties of EFG tensors are as specified in the legend to Fig. 2 (*3*), are -64.3, 81.3, and -15.9 kHz, respectively. The discrepancies between these two sets of estimates can be explained in terms of small deviations, by no more than 1°, of the relevant EFG axes from the tetrahedral directions.

K, the fits were sensitive to w so that this parameter was optimized; the corresponding standard errors were of the order of a few hertz, that is, very small in comparison wit the values of w which for both orientations vary in the limits of 1700–1950 Hz. For each orientation, the optimized values of w come in pairs. Within each pair, the difference between these values is of the order of the corresponding standard errors while the differences between the pairs can reach as much as 200 Hz. A closer look at these results reveals that each such pair corresponds to the experiments performed at exactly the same setting of the goniometer (the given orientation of the sample, I or II, was always left unchanged when passing to the next temperature). The rotation axis may slightly deviate from the direction of the monoclinic axis, which may render the two CD_3 groups in elementary cell slightly nonequivalent. Thus, the scattering of the results for w may simply reflect imperfect reproducibility of the goniometer settings or, in other words, imperfect reproducibility of these small deviations from equivalence. In handling the data at higher temperatures, the magnitude of w was kept fixed, equal to the average of the values estimated at lower temperatures.

For orientation II, the magnitude of $|\alpha|$ is smaller by some 25% than for orientation I. As the splittings of the β lines are proportional to $|\alpha|^2$, one could expect that the relevant information would be more readily extractable from the spectra measured for orientation I than for orientation II. For reasons which will be discussed later on, the real situation has proven to be quite the reverse. Fully consistent results could be obtained only for orientation II. Selected examples of the fits obtained for the latter are displayed in Figs. 3 and 4. The quality of the remaining fits for orientation II is similarly good. The estimates of the quantities Δ, k_K, and k_t describing the dissipative tunneling are collected in Table 1.

The spectra in Fig. 3 are representative for the low-temperature region where the spectral pattern is dominated by coherent tunneling and the dissipative processes are slow relative to $|\alpha|$. Despite the fact that for orientation II the β lines show relatively poor fine structures at low temperatures, the information about the interesting system parameters, contained in the whole sets of FID and QE spectra, has proven to be nearly complete. At each of the three temperatures where the α lines are still resolved (22, 24, and 26 K in our case), the fitting procedure delivers also estimates of the effective quadrupolar coupling constants q_A, q_B, and q_C. A comparison of the present results for the quadrupolar coupling constants with the values determined previously (*3*) is made in the legend to Fig. 3.

It follows from the considerations of the Theory section as well as from the lineshape simulations that for orientation II the low-temperature spectra should be relatively insensitive to the rate constant $k' = k_t - k_K$ of the nonclassical jumps. Indeed, an inclusion of k' into the set of the fitted parameters does not lead to a reduction of the overall rms error by more than 0.5%; in general, the optimized value of k' proves to be dependent on the assumed initial value. The estimates of the remaining parameters, obtained at convergence under assumption of $k' =$

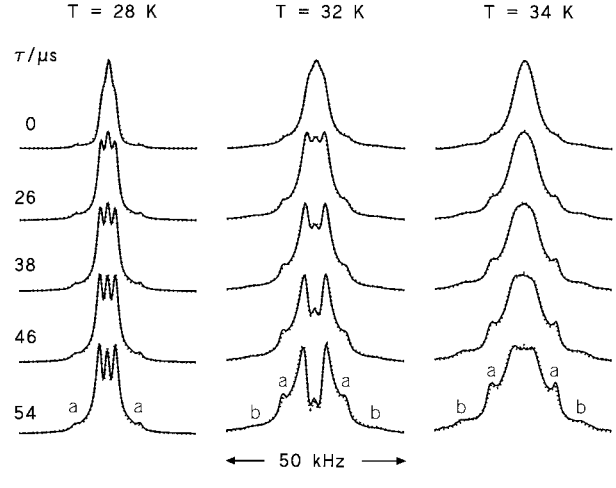

FIG. 4. Selected experimental QE spectra (solid lines) and the corresponding theoretical "best fit" spectra (dotted lines) for the displayed values of echo time for orientation II at the temperatures where the α lines are no longer visible. The values of the effective quadrupolar coupling constants q_A and q_B, -64.6 and 83.6 kHz, respectively, which are the averages of the results obtained from the spectra at temperatures 22–26 K, were not optimized. Note a second impurity doublet, *b*, now emerging in the spectra at long echo times.

TABLE 1
Results of Iterative Lineshape Analysis of FID and QE Spectra for Orientation II[a]

T/K	Δ/MHz	k_K/1000 s^{-1}	k_t/1000 s^{-1}	Δ/MHz	k/1000 s^{-1}
22	2.293 ± 0.005	13.9 ± 0.1	—	2.10[b]	13.0[b]
24	2.004 ± 0.003	26.9 ± 0.1	—	1.89	28.5
26	1.610 ± 0.004	68.9 ± 0.4	—	1.62	75.5
28	1.324 ± 0.001	172 ± 2	335 ± 5	1.38	300
30	1.088 ± 0.001	542 ± 6	670 ± 11	1.13	660
32	0.865 ± 0.001	1660 ± 5	1720 ± 10	0.87	1400
34	0.663 ± 0.002	3990 ± 21	2800 ± 35	0.76[b]	3110[b]

Note. In the last two columns, the corresponding results of Ref. (5), where only the pseudo-classical process was taken into account, are displayed.
[a] Standard errors are given.
[b] Unpublished.

0, remain practically unchanged when k' also is allowed to vary. In our previous analysis, based on a visual comparison of the simulated and experimental FID spectra, where only the pseudo-classical process was taken into account, the values of its rate constant, k, determined at temperatures up to 26 K are in good agreement with the corresponding values of k_K determined currently (see Table 1).

Above 26 K, the α lines coalesce and further undergo a gradual narrowing, while the multiplet structure of the $\pm\beta$ resonances becomes more and more apparent. The spectra no longer contain sufficient information about the magnitudes of all three quadrupolar coupling constants. In our calculations involving the spectra at temperatures above 26 K, only one of the latter was treated as a free parameter, the one that was determined from the low-temperature spectra with the least accuracy. The same involves the calculations for orientation I.

Along with increasing resolution of the $\pm\beta$ multiplets, and, therefore, a growing contribution of the *EA* and *AE* transitions to the β multiplet, the spectra ought to be increasingly sensitive to the possible occurrence of nonclassical jumps. For orientation II, our results derived from the experiments above 26 K confirm these predictions. For instance, for the series of spectra measured at 28 K the overall rms error drops by about 8% when the parameter k' ($= k_t - k_K$), initially kept equal to zero, is then allowed to vary. The differences between the "best fit" QE spectra calculated for k' fixed at zero and those with k' treated as adjustable parameter are shown in Fig. 5. Compared with the experimental spectra (middle column in Fig. 5), the former exhibit as a small but systematic deviation involving the amplitude of the central peak. This deviation disappears when the parameter k' is also optimized. In the work mentioned above concerning the FID spectra, where only the pseudo-classical process was taken into account (5), the value of its rate constant, k, at 28 K, was found to be 3.0×10^5 s^{-1}. It is therefore nearly twice as large as the value of k_K determined currently but it is close to k_t (see Table 1). Also, at temperatures above 28 K, the previous values of k generally fall closer to the values of k_t than to those of k_K (see Table 1). In order to rationalize this somewhat puzzling observation, we performed simulations of FID and QE spectra using the complete Eq. [1] and its approximate version in which the nonclassical dissipative term was neglected. The latter will further be referred to as the AB equation. The main inference from these simulations is that the adjustment of the single rate parameter, k, in the AB equation to get a fair reproduction of the exact lineshape functions is critically dependent on the status of the α lines in the calculated spectra. When these lines are clearly visible, similarity is achieved when k is put equal to k_K. When the α lines collapse, using a visual similarity as the criterion of the fit quality, one will concentrate at the best possible reproduction of the β multiplets which become then a dominating element of the lineshape. This will be achieved when k is put equal to k_t, provided that k_K and k_t are of the same order of magnitude.

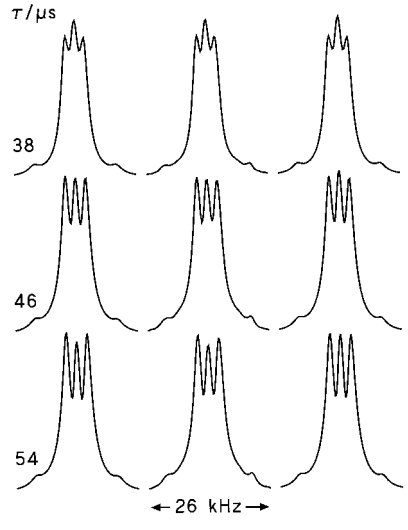

FIG. 5. A comparison of selected experimental QE spectra at 28 K (middle column) with the corresponding theoretical "best fit" spectra obtained with (left column) and without (right column) taking into account of the nonclassical dissipative term in the lineshape equation. The values of the single rate parameter, k, and Δ, obtained in the latter calculations, are $(2.06 \pm 0.02) \times 10^5$ s^{-1} and 1.320 ± 0.001 MHz, respectively. The systematic deviation in the theoretically reproduced amplitude of the central peak, visible in the spectra in the right column, is absent from the spectra in the left column.

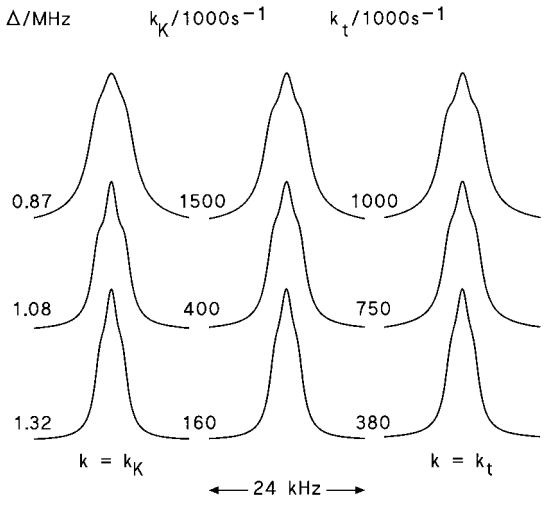

FIG. 6. Theoretical FID spectra for orientation II calculated for the displayed values of Δ, k_K, and k_t (middle column) and the corresponding spectra calculated using the AB equation with the single rate parameter k equal to k_K (left column) and to k_t (right column). Note a striking similarity of the exact lineshape functions to the corresponding approximate functions displayed in the right column. For the assumed values of k_K the broad background signals for which there are discrepancies are nearly invisible (see text).

Figure 6 illustrates typical situations that may be encountered when FID spectra of our crystal in orientation II, in the temperature range where the α lines are collapsed, are considered. It is understandable that the discrepancies that may occur for the barely visible α lines when k is drifted far from k_K can easily be sacrificed for the benefit of improved reproducibility of the dominating pattern. These observations explain why our previous estimates of k fall close to k_K in the low-temperature region while they shift toward k_t in the temperature range where the α lines are nearly invisible. In the experimental spectra of the system considered, a sudden collapse of the α lines occurs on passing from 26 to 28 K. We can therefore rationalize our former observation of an unexplicable jump of k by a factor of 4 when the temperature is raised from 26 to 28 K, followed by a jump by only a factor of 2 upon further increasing the temperature by 2 K, which we left uncommented on in Ref. (*5*).

It must be added that for temperatures above 26 K the results of our former visual fits are not reproduced either by the iterative fits based on the AB equation (such fits were always performed at the penultimate stages of our iterative analyses). This fact seems to contradict the arguments invoked above. However, unlike the human eye, the minimization algorithm is sensitive to the possible discrepancies occurring for the remnants of the collapsed α lines. At the temperatures of 28 and 30 K, an optimization of the single rate parameter delivers values that fall closer to the corresponding values of k_K rather than to those of k_t. As can be seen in the right part of Fig. 5, the propensity to maintain a fair fit of the (very small, but represented by a large number of experimental points) background signal leads to a worsened reproduction of the dominating β multiplet. Only at 34 K does the iterative algorithm based on the AB equation happen to reproduce the results of our former visual fits.

In Fig. 7, selected best fit spectra obtained in these calculations are compared with the corresponding experimental spectra and with the best fit spectra obtained using the complete lineshape equation (which are also displayed in Fig. 4). For the latter fits, the overall rms error is smaller than for the former by about 9%. These results are remarkable due to the fact that they seem to document the nonexistence of any "classical limit" in the dissipative behavior of the CD_3 rotor investigated currently: Inspection of the trends in the temperature dependences of k_K and k_t, visualized in Fig. 8, allows one to predict that at still higher temperatures these quantities will further diverge.

For orientation I, the magnitude of α is close to its conditional maximum over all the orientations conforming to the monoclinic symmetry (for which the CD_3 groups are magnetically equivalent). For this orientation, the spectra were measured also at 17 K. The lineshape fits for the latter experiment are shown in Fig. 9. The quality of these fits is not as good as that for the experiments at orientation II, which in part may be due to the fact that at this low temperature only two steps of the otherwise four-step phase cycle could be performed, because of very long relaxation time. Unlike for orientation II, the spectra are sensitive to the intramolecular dipole–dipole couplings between the deuterons. The optimized dipole–dipole coupling constant obtained at 17 K, assuming perfect threefold symmetry of the methyl group, amounts to 820 $\pm$ 13 Hz (the corresponding theoretical value, calculated for the standard geometry, is 1000 Hz). Estimates of the relevant system parameters are listed in the legend to Fig. 9. Note that at this

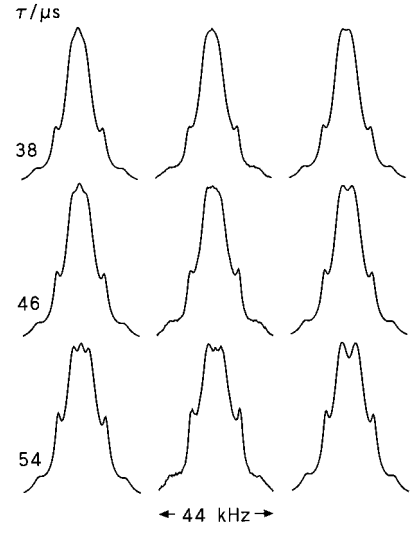

FIG. 7. Same as Fig. 5, but for the temperature of 34 K. The values of the single rate parameter, k, and Δ, obtained in the calculations with the neglect of the nonclassical dissipative term (the spectra in the right column), are $(2.9 \pm 0.1) \times 10^5$ s^{-1} and 0.741 $\pm$ 0.003 MHz, respectively.

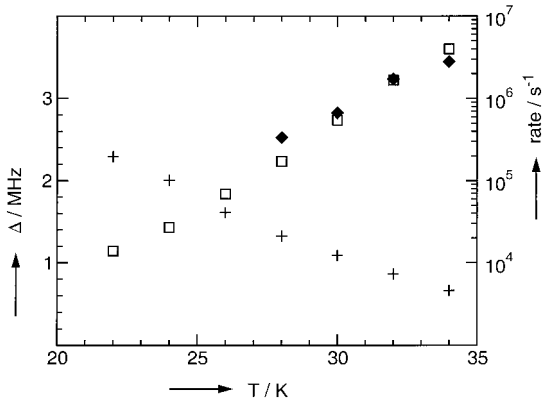

FIG. 8. Temperature dependence of the results of the lineshape analysis given in Table 1. Left scale: tunneling frequency Δ (crosses). Right scale: rate constants k_K (open squares) and k_t (full diamonds). For all values, the associated standard deviations are too small to be visible on the scale of the figure. The tunneling frequency decreases almost linearly towards zero with increasing temperature, while the rate constants exhibit a roughly exponential temperature dependence. The Arrhenius plot of $k_K(T)$ (not shown) exhibits substantial deviation from linearity in the low-temperature limit. The differences between k_K and k_t indicate the occurrence of a dissipative process without classical analog (c.f. Eq. [3]). Note that at 28 K, k_K and k_t differ by almost a factor of 2.

relatively low temperature the dissipation via pseudo-classical jumps has not been frozen out. The underlying dissipation mechanism is probably due to the incoherent tunneling concerned with activation to the first excited torsional state (*9, 10*). The possible impact of the nonclassical jumps on the lineshapes could not be detected.

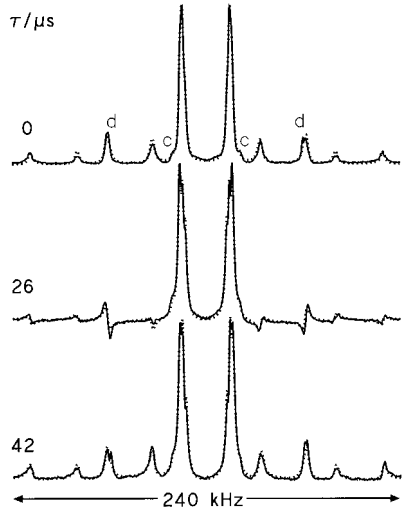

FIG. 9. Same as Fig. 3, but for orientation I at the temperature of 17 K. The labels *c* and *d* mark impurity doublets (see text). The optimized values of Δ and k_K are 2.538 ± 0.007 MHz and 7600 ± 140 s^{-1}, respectively. The optimized values (in kHz) of the effective quadrupolar coupling constants q_A, q_B, and q_C are −88.2 ± 0.3, 130.6 ± 0.3, and 16.4 ± 0.6, respectively. For the pertinent orientation parameters Θ and ϕ listed in the legend to Fig. 2, the values calculated from the previous estimates (*3*) (see legend to Fig. 3) are −85.0, 131.8, and 14.0 kHz, respectively.

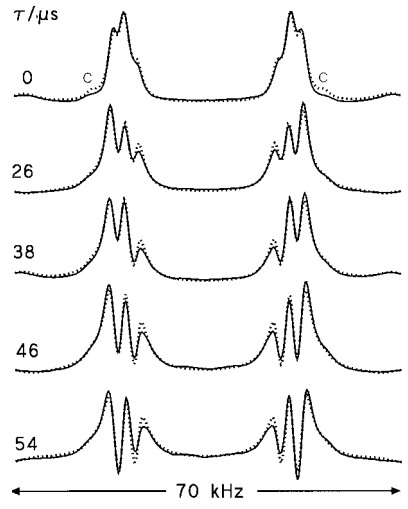

FIG. 10. Same as Fig. 9, but for the temperature of 24 K, and only the central parts (the β multiplets) are shown. Now the impurity doublet *c* almost completely overlaps with the outermost components of the β multiplets. The optimized values (in kilohertz) of the effective quadrupolar coupling constants q_A, q_B, and q_C are −87.0 ± 0.2, 130.9 ± 0.2, and 15.8 ± 0.4, respectively.

For the spectra measured at 22, 24, and 26 K (where the α lines remain still resolved), the fitting procedure has failed to reproduce the lineshapes of the β lines with an equally good accuracy as for orientation II. Only for the α lines do the fits remain good. Fits of the central part of the spectra at 24 K are shown in Fig. 10. Just at this temperature the dissimilarity between the experimental and theoretical spectra seems to reach its maximum. In general, fits of such a quality as in Fig. 10, obtained for solid-state NMR spectra, would probably be considered more than satisfactory. However, in the present context, where the focus is on details, one may start wondering about possible flaws in the theory and/or experiment to be blamed for these discrepancies. A deeper discussion of the possible reasons of the latter seems thus indispensable.

When analyzing the spectra for orientation II, we had already to worry about impurity signals. For that orientation, it is a fortunate circumstance that the most intense of such signals, forming a typical static doublet, happens to occur outside the region of the β resonances (see Figs. 3 and 4). The other impurity signals, which become visible only at higher temperatures (e.g., the broad doublet marked "*b*" in Fig. 4), are probably due to a small admixture of isotopomers with partially protonated methyl groups. The spectral properties of such isotopomers of acetylsalicyclic acid were the subject of separate studies (*22, 23*). Their rotation patterns are also known (*21*). Due to the dependence on orientation of the intragroup dipolar couplings to the methyl protons, the widths and, thereby, the amplitudes of the ^{2}H resonances in such isotopomers can differ considerably for different orientations. With increasing temperatures, these resonances undergo motional broadening, coalescences, and, ultimately, motional narrowing; following the angular dependence of the quadrupolar

splittings, these lineshape effects are also strongly dependent on the orientation.

Taking all this into account and making use of the above-mentioned rotation patterns, we can interpret the impurity signal marked *d* in Fig. 9 as arising from the deuterons occupying position *A* in the isotopomers CHD_2. As can be seen from the corresponding rotation patterns, the signals of the deuterons at position *C* in this isotopomer must occur in the region of the β lines; the overall integral intensity of this hidden signal is about twice as large as that of *d*. There may also be a small admixture of the isotopomer CH_2D, the traces of which have probably been detected previously for still different orientations of the same crystal sample (*4*). One of the signals of the latter, the one whose integral intensity increases with temperature (*22*), would coincide with the outermost components of the β pattern. It is this signal that may be responsible for the apparent amplitude increase of these components, which is clearly visible in Fig. 10. The minimization procedure then tries to compensate such a deformation at the cost of the worsened fit of the inner components. All of this must in turn impose some bias on the estimates of the system parameters. This is the circumstance which we could not properly assess when starting our calculations for orientation I.

In orientation II, in the low-temperature limit, all of these signals fall far in the wings and are substantially broadened by the intragroup dipolar interactions with protons. Because, additionally, in orientation II all of the individual signals of the CD_3 group are twice as intense as in orientation I, all of these impurity signals are too small to be observed until at elevated temperature they coalesce into one doublet, that marked *b* in Fig. 4.

The origin of the impurity signal labeled *a* in Fig. 3 and 4 remains, however, unknown. On the other hand, the signals labeled *c* in Figs. 9–11 may be due to a small fraction of deuterons which substitute protons in the carboxylic groups (*21*). Unlike the case of the impurities from the partially protonated isotopomers, the bias due to the presence of the *c* signals was to some extent neutralized in the calculations for orientation I. The parameters of this signal determined at temperatures of 17 and 22 K were used in the analyses of spectra at the temperatures where it completely overlaps with the signals of interest.

Despite the fact that the results obtained for orientation I are generally biased, it seems instructive to compare them with the results for orientation II which seem to be free of such a bias and can therefore be regarded as accurate. Because in interpreting the spectra of tunneling CD_3 groups one will always face interferences with admixtures of unwanted isotopomers, one must be aware of the possible limits of accuracy, regardless of whether the fits are obtained by a visual comparison or in an automated iterative process.

For temperatures up to 26 K, the values of k_K, the evaluation of which is based mainly on the features of the α lines, are in a perfect agreement, to within the respective standard errors,

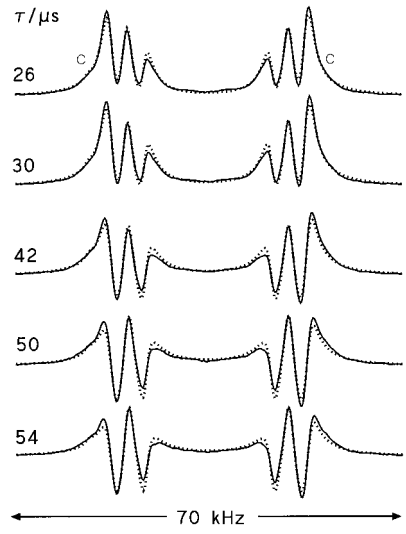

FIG. 11. Same as Fig. 10, but for the temperature of 28 K. The impurity doublet *c* is now hidden under the outermost components of the β multiplets. The FID spectrum was not included in the analysis because of baseline distorsions. The values of the effective quadrupolar coupling constants q_A and q_B, −86.6 and 131.0 kHz, respectively, which are the averages of the results obtained from the spectra at temperatures 17–26 K, were not optimized.

with those obtained for orientation II (see Table 1). The values of Δ, the information on which is contained in the β pattern, are smaller by 5–10% than those determined for orientation II. For the temperatures of 28–34 K, the values of Δ are nearly identical, to within three standard errors, with those obtained for orientation II (at 28 and 30 K the FID spectra had to be excluded because of substantial baseline distortions originating from very broad resonances of coalesced α lines). It is remarkable that the scattering of the results for Δ is practically the same as in our previous studies based on a visual comparison of the experimental and simulated FID spectra (*3*).

For orientation I, optimization of $k' = k_t - k_K$ is technically feasible already at 22 K (here $|\alpha|$ is about 1.25 times greater than for orientation II). However, at temperatures of 22, 24, and 26 K, the values of k' obtained at convergence are probably biased by lineshape distortions due to the impurity signals. The corresponding values of k_t seem to be overestimated and, moreover, their temperature behavior is counterintuitive: the value of k_t obtained at 26 K, of about $2.0 \times 10^5\ s^{-1}$, is *smaller* than the corresponding quantity at 22 K, $2.9 \times 10^5\ s^{-1}$. On the other hand, at 28 K the bias seems less severe since the estimates of both k_K and k' at 28 K are in a fair agreement with their counterparts determined for orientation II, namely k_K^I (28 K) = $(1.53 \pm 0.04) \times 10^5$ and k_t^I (28 K) = $(3.06 \pm 0.07) \times 10^5\ s^{-1}$. Selected examples of the fits at 28 K are shown in Fig. 11. The somewhat better quality of these fits compared to those at 24 K is probably due to the fact that the motionally averaged signals of the CH_2D and CHD_2 isotopomers, which must occur somewhere in the region of the β signals, are considerably broadened at this temperature. At still higher temperatures, the

signals of the CH_2D isotopomer probably undergo motional narrowing; its averaged signal can be expected to occur still in the β region. A growing amplitude of the latter may again pose an offense to the lineshapes of the signals of interest. In consequence, in comparison with the corresponding values determined for orientation II (see Table 1 and Fig. 8), above 28 K the optimized values of k_K and k_t behave less smoothly with temperature.

The simple model of rotor–bath interactions introduced previously (*10*) affords a consistent, although only semiquantitative, description of the temperature dependences of Δ, k_K, and k_t in terms of only a few adjustable parameters. The values of the latter were determined in Ref. (*10*) on the basis of our earlier data for Δ and the single rate parameter (*3, 5*). Our attempts to refine the estimates of the model parameters by confronting them with the more complete data displayed in Table 1 did not lead to a substantial improvement of the fit. Our present aim is to modify the model in two aspects: (i) to refine the torsional potential according to a recent INS study on the protonated compound (*24*) and (ii) to replace the linear rotor–phonon coupling by a more realistic interaction model. Our present low-temperature data on k_t, which we could obtain only from the spectra in orientation I, may be unreliable. We therefore intend to carry out additional NMR experiments, aimed at observing the weak off-resonance signals in the frequency regions around $\pm\Delta$, whose widths could provide a direct measure of k_t. Our general aim is to demonstrate that, in the studies on damped quantum rotation, NMR spectroscopy can play exactly the same role for deuterated species as does INS spectroscopy for protonated species.

CONCLUSIONS

We have shown that the wealth of information about damped quantum rotation of CD_3 groups, contained in QE spectra, can be fully explored in a broad temperature range, provided that the impact of admixtures of incompletely deuterated isotopomers can be accounted for. In our present research, the latter condition was met for one orientation of the crystal in the external magnetic field. For this orientation, we could demonstrate that the recently proposed lineshape equation, which apart from the familiar Alexander–Binsch term contains an additional dissipative term, is capable of describing even subtle details of the spectra. We have obtained preliminary evidence of the occurrence of this novel dissipative mechanism in the system studied. Our results seem to suggest that there is no classical limit in the dissipative behavior of the system studied.

ACKNOWLEDGMENTS

This work was sponsored in part by the Polish Committee for the Advancement of Research (KBN) under Grants 3 T09A 062 12 and 2 P03B 074 15.

REFERENCES

1. A. J. Horsewill, *Prog. Nucl. Magn. Reson. Spectrosc.* **35,** 359 (1999).
2. T. Bernhard and U. Haeberlen, *Chem. Phys. Lett.* **186,** 307 (1991).
3. A. Detken, P. Focke, H. Zimmermann, U. Haeberlen, Z. Olejniczak, and Z. T. Lalowicz, *Z. Naturforsch.* **50A,** 95 (1995).
4. Z. Olejniczak, A. Detken, B. Manz, and U. Haeberlen, *J. Magn. Reson. A* **118,** 55 (1996).
5. S. Szymański, Z. Olejniczak, and U. Haeberlen, *Phys. B* **226,** 161 (1996).
6. A. Detken, P. Schiebel, M. R. Johnson, H. Zimmerman, and U. Haeberlen, *Chem. Phys.* **238,** 301 (1998).
7. A. Detken, H. Zimmermann, and U. Haeberlen, *Mol. Phys.* **96,** 927 (1999).
8. Z. T. Lalowicz, U. Werner, and W. Müller-Warmuth, *Z. Naturforsch. A* **43,** 219 (1988).
9. A. Heuer, *Z. Phys. B Condens. Matter* **88,** 39 (1992).
10. S. Szymański, *J. Chem. Phys.* **111,** 288 (1999).
11. I. Solomon, *Phys. Rev.* **110,** 61 (1958).
12. A. Hewson, *J. Phys. C* **15,** 3841 (1982); *ibid.* **15,** 3855 (1982).
13. A. Würger, *J. Phys. Cond. Matter* **1,** 6901 (1989); *Z. Phys. B Condens. Matter* **76,** 65 (1989).
14. M. Prager and A. Heidemann, *Chem. Rev.* **97,** 2933 (1997).
15. F. Apaydin and S. Clough, *J. Phys. C Ser. 2* **1,** 932 (1968); S. Clough, *in* "NMR. Basic Principles and Progress," Vol. 13, (P. Diehl, E. Fluck, and R. Kosfeld, Eds.), p. 113, Springer-Verlag, Berlin, 1976.
16. S. Alexander, *J. Chem. Phys.* **37,** 974 (1962).
17. G. Binsch, *J. Am. Chem. Soc.* **91,** 1304 (1969).
18. A. Würger and A. Hüller, *Z. Phys. B Condens. Matter* **78,** 479 (1990).
19. A. Würger and A. Heidemann, *Z. Phys. B Condens. Matter* **80,** 113 (1990).
20. P. J. Wheatley, *J. Chem. Soc.* **1964,** 6036.
21. A. Detken, Ph.D. Thesis, University of Heidelberg, 1998.
22. A. Detken and H. Zimmermann, *J. Chem. Phys.* **109,** 6791 (1998).
23. A. Detken and H. Zimmermann, *J. Chem. Phys.* **108,** 5845 (1998).
24. M. R. Johnson, B. Frick, and H. P. Trommsdorff, *Chem. Phys. Lett.* **258,** 187 (1996).